Improved PCA Methods for Process Disturbance and Failure Identification

Amir Wachs and Daniel R. Lewin
Wolfson Dept. of Chemical Engineering, Technion, I.I.T., Haifa 32000, Israel

Principal component analysis (PCA) is a powerful technique for constructing reduced-order models based on process measurements, obtained by the rotation of the measurement space. These models can be subsequently utilized for chemical-process monitoring, particularly for disturbance and failure diagnosis. Since the standard PCA procedure does not account for the time-dependent relationships among the process variables, this leads to poorer disturbance isolation capability in dynamic applications. A simple idea, in which the last s PCA scores are recursively summed and used to construct descriptive statistics for process monitoring, is presented. Analytically, it is shown that the disturbance resolution afforded is enhanced as a result. Resolution is improved further through the use of an algorithm that enhances the correlations between the input and output variables through optimal time shifting. An overall strategy for on-line monitoring developed includes disturbance identification through mapping. The approach is demonstrated by two industrially relevant case studies.

Introduction

With the advent of improved instrumentation and automation, chemical processes now produce large volumes of information. However, in the absence of appropriate processing, only limited knowledge can be extracted directly from these data, with many abnormal events, relating to interactions between the variables, remaining undiscovered. Several multivariate statistical methods have been developed to identify correlations between the variables and create a new array of orthogonal axes that capture most of the variability in the collected information (such as Mardia et al., 1982; Martens and Naes, 1989; Jackson, 1989; Wise et al., 1990; Kresta et al., 1991). One of the most commonly used method is principal component analysis (PCA), which also has been applied to industrial processes (such as Kosanovich et al., 1996; Sanetan et al., 1997). This method effectively reduces the original measurement space, and as a result, facilitates process failure and disturbance diagnosis, since the reduced-order model so derived captures the essential correlations between the process variables that characterize normal operating conditions (NOC). Deviations from these relationships, as a consequence of the effect of failures or disturbances, are then in general easier to detect (Dunia and Qin, 1998). However, the basic PCA method has difficulty in isolating deviations from normal operating conditions when shifts are relatively small. Moreover, the PCA method ignores the sequential dependencies in the samples, and thus neglects valuable characteristics that can be used to increase failure detection resolution.

The main novelty of the approach introduced in this article and described in the following section, is the use of the so-called summed-scores construct, in which descriptive statistics are computed using a vector of the last *s* PCA scores. Since it can be expected that disturbances propagate in a dynamical system with a given directionality, the summed-scores construct leads to a reinforcement of this directionality, and thus improves the disturbance detectability. Basically, the summed-scores approach is an extension of the standard univariate moving-average technique, to the multidimensional space of scores, obtained from applying the PCA model.

Two techniques related to the moving average are the cumulative sum (CUSUM) and the exponential weighted moving average (EWMA). Each of these has advantages and disadvantages compared to the others, as has been discussed thoroughly in the univariate statistical literature (such as Montgomery, 1991). The main disadvantage associated with

Correspondence concerning this article should be addressed to D. R. Lewin.

applying the CUSUM is that the resulting statistics are then not normally distributed, thus leading to problems in the interpretation of the results obtained. An important consideration when considering the application of MA or CUSUM over EWMA is that the latter is more complicated to implement. By opting for moving-average techniques, one avoids the added complexity of tuning a filter time constant (for each channel), as well as its rather arbitrary effect on the performance obtained (Ogunnaike and Ray, 1994). It should be pointed out that the characteristics of the CUSUM, MA, and EWMA approaches remain when applying the methods on uncorrelated, multidimensional data. The application of a CUSUM chart in conjunction with PCA was suggested by Zhang et al. (1996), while Wold (1994) utilized the EWMA on scores data.

It is worth noting that special methods must be used to apply PCA efficiently to processes characterized by time-varying trajectories (Wold et al., 1987; Wachs and Lewin, 1998). An algorithm introduced here, which accounts for the dynamic delay between variables, is the so-called delay-adjusted PCA (DAPCA). This approach has similarities with that proposed by Ku et al. (1995), in which the dynamic behavior of the process is treated, but not its delays. In DAPCA, the most appropriate time delays between the input and output trajectories are determined by shifting input variables backward iteratively until the correlation between each output and each shifted input is maximized. In the third section, this technique is shown to improve the resolution of PCA. The overall algorithm, incorporating both the summed-scores construct and delay adjustment, is presented in the fourth section. The algorithm is tested on a simulated CSTR for disturbance diagnosis in the fifth section, where delay-adjustment is not used.

Relatively little has been published on the use of the scores plane as a fault-identification tool (Kresta et al., 1991; Lewin, 1995; Raich and Cinar, 1996; Dunia and Qin, 1998). By moving the cluster of shifted data further away from NOC, the summed-scores statistics lead to a reduction in the crossing zone in the NOC envelope, and thus improves the ability to map common disturbances and to identify them. The ability of PCA to provide visualization of abnormal conditions is limited in practice to problems that can be adequately represented by three principal components at most. In circumstances where more than three principal components are needed, either measures must be adopted which account for deviations in all dimensions of the problem space (such as Hotelling's T^2 statistics), or multidimensional visualization methods can be applied (Wachs et al., 1999). An attractive alternative is the so-called "decentralized PCA" (Georgakis et al., 1996), in which the data set is divided into smaller groups, each associated with a subsection of the process. This requires additional computational effort, but has important advantages in that the mapping of outliers is carried out with a higher degree of specificity and sensitivity. An example application of this idea for on-line monitoring is given in the sixth section.

s-Summed Construct and PCA

Consider the univariate moving-average filter (Montgomery, 1991): Let $x_1, x_2, \ldots, x_t, \ldots$ denote a sequence of samples. Then, the moving average of span w at time t is defined as

$$M_t = \frac{x_t + x_{t-1} + \cdots + x_{t-w+1}}{w}. \quad (1)$$

Assuming normal distribution (that is, no serial correlation in the sequence), the variance of the moving average M_t is

$$V(M_t) = \frac{1}{w^2} \sum_{i=t-w+1}^{t} V(x_i) = \frac{1}{w^2} \sum_{i=t-w+1}^{t} \sigma^2 = \frac{\sigma^2}{w}. \quad (2)$$

Thus, the expected standard deviation is $\sigma/\sqrt{w}$. However, if sequential correlation exists, the standard deviation of the moving-averaged data, σ^*, will be higher. To illustrate this, consider the serially correlated sequence:

$$y_i = \alpha \cdot y_{i-1} + (1-\alpha) \cdot x_i, \quad (3)$$

where x_i is white noise. Figure 1 shows the dependency of the ratio $\sigma^*/(\sigma/\sqrt{w})$ on the degree of serial correlation of y_i, as brought by α, with $w = 10$.

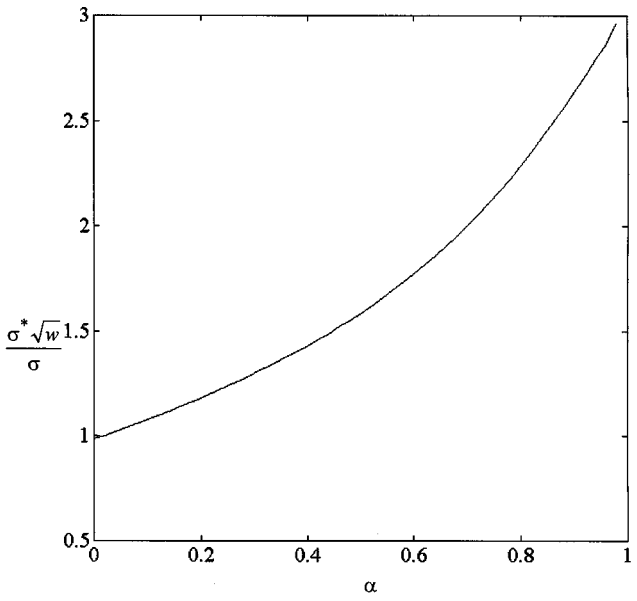

Figure 1. Ratio of the actual and ideal standard deviations as a function of the degree of sequential correlation.

In the standard moving-average technique, control limits of $\sigma/\sqrt{w}$ are used in any case, which therefore increases the false-alarm rate when applied to serially correlated data. When sequential correlation exists, the average run length (ARL) will be reduced in proportion to α. More robustly, σ^* is used instead to construct control limits, and consequently, the sensitivity to false alarms is similar to that of using the raw data, with only the resolution-enhancement affected. As $\alpha \to 1$ ($y_i \to y_{i-1}$), fault-resolution becomes similar to that attained using standard Shewart control charts.

When calculating the corresponding control limits, applying the moving-average technique on multidimensional data

requires taking into account the correlation that exists among the variables. In the transformation of the multidimensional space of raw data into an uncorrelated space of principal components, each principal component acts as an independent variable, and thus the characteristics of the moving average remain the same for each of the principal components.

Definition. Consider the data sequence $X = [x_1, x_2, \ldots, x_n]$, with $n \gg 1$. For simplicity, a one-dimensional example is treated, but its extension to multidimensional data is trivial. Assuming the data are normally distributed and scaled to have mean zero and unit standard deviation, and also that every subset of sequential samples from the full data set has a normal distribution, one can form the *s-summed construct,* $\tilde{X}$, which is a vector of $n - s$ values defined as

$$\tilde{x}_i = \sum_{k=i-s+1}^{i} x_k \qquad i = s, \ldots, n. \tag{4}$$

Theorem 1. The *s*-summed construct, $\tilde{X}$, defined in Eq. 4, is of mean zero and of standard deviation $\sqrt{s}$.

Proof. Since X has zero mean and unit standard deviation, $E(X) = 0$ and $\sigma^2(X) = 1$. Consequently,

$$E(\tilde{X}) = E(X_{i-s} + X_{i-s+1} + \cdots + X_i) = E(X_{i-s}) + E(X_{i-s+1}) + \ldots + E(X_i) = 0 + 0 + \ldots + 0 = 0.$$

Furthermore,

$$\sigma^2(\tilde{X}) = E(\tilde{X}^2) - \left[E(\tilde{X})\right]^2 = E(\tilde{X}^2) - 0$$

$$= E\left(\left[X_{i-s} + X_{i-s+1} + \cdots + X_i\right]^2\right)$$

$$= E\left(\left[X_{i-s}\right]^2\right) + E\left(\left[X_{i-s+1}\right]^2\right) + \cdots + E\left(\left[X_i\right]^2\right) + 2 \cdot \left[E(X_{i-s} \cdot X_{i-s+1}) + \cdots + E(X_{i-1} \cdot X_i)\right]$$

$$= \sigma^2(X_{i-s}) + \sigma^2(X_{i-s+1}) + \cdots + \sigma^2(X_i) + 2 \cdot \left[E(X_{i-s}) \cdot E(X_{i-s+1}) + \cdots + E(X_{i-1}) \cdot E(X_i)\right]$$

$$= 1 + 1 + \cdots + 1 + 2 \cdot (0.0 + \cdots + 0 \cdot 0) = s$$

$$E(\hat{X}) = E(X_{i-s} + X_{i-s+1} + \cdots + X_i) = E(X_{i-s}) + E(X_{i-s+1}) + \cdots + E(X_i) = 0 + 0 + \cdots + 0 = 0.$$

Thus, $\tilde{X}$ has zero mean and is of standard deviation $\sqrt{s}$.

Properties. If the sequence X is disturbed by a step change of δ imposed at instance j, then the disturbed sequence, X^D, is defined as

$$x_i^D = \begin{cases} x_i, & i < j \\ x_i + \delta, & i \geq j. \end{cases} \tag{5}$$

The *s*-summed sequence $\tilde{X}^D$ derived from X^D exhibits a ramped change of α each instant over s instances, starting at instant j. Thus, while the standard deviation of $\tilde{X}$ is a factor of $\sqrt{s}$ bigger than that of X, the shift in $\tilde{X}^D$ is a factor of s bigger than that of X^D. Consequently, there is an increase by $\sqrt{s}$ in the resolution between shifted data and normal limits. As discussed before, the increase in resolution is dependent on the degree of sequential correlation. In practice, the resolution enhancement lies between 1 and $\sqrt{s}$.

Summed-scores PCA

Here, the idea of the *s*-summed construct is integrated into PCA (SSPCA). This is best introduced using an example.

Example 1. For demonstration purposes, consider a process having two, linearly correlated sensors:

$$X_1 = \phi \tag{6}$$

$$X_2 = a\phi + b. \tag{7}$$

Assuming the measurements are normally distributed at NOC, then after scaling the data to have mean zero and unit variance (autoscaling), the scaled data from the two sensors are the same: $\hat{X}_1 = \hat{X}_2$. Following the PCA procedure, the data set is projected onto a new set of orthogonal axes that are the eigenvectors of the correlation matrix of the scaled data, corresponding to the variability of measurements relative to their associated eigenvalues:

$$X = \left[\hat{X}_1, \hat{X}_2\right] \tag{8}$$

$$A = \frac{X^T X}{n-1} = P^T \Lambda P \tag{9}$$

$$T = XP. \tag{10}$$

For the given example, the eigenvectors corresponding to the eigenvalue in Λ, $\lambda_{1,2} = 2, 0$, are $p_{1,2} = [\sqrt{0.5}\ \sqrt{0.5}]^T, [\sqrt{0.5}\ -\sqrt{0.5}]^T$. From this result, it can be concluded that the first principal component vector captures the entire data variance (that is, the scores matrix, T, has one vector of zeros, and thus, the second principal component can be neglected with zero residual). The *s*-summed construct is computed, giving the so-called *Summed-scores PCA:*

$$\tilde{t}_{1,i} = \sum_{k=i-s+1}^{i} t_{1,k}, \qquad i = s, \ldots, n. \tag{11}$$

Following Theorem 1, $\tilde{T}_1$ has a normal distribution, which is of zero mean and of standard deviation $\tilde{\sigma}$. The NOC boundaries are determined to be at $\pm 3 \cdot \tilde{\sigma}$ from the origin, so 99.7% of NOC data will lie within the NOC limits.

To demonstrate the difference in detection and steady-state resolution of a change in operating conditions, assume that a process change, causing a shift of slightly more than 3σ, propagates following a first-order lag with a time constant of ten times the sampling interval. If the diagnosis is carried out using conventional PCA, the 3σ limits, delineating the NOC, will be crossed due to the shift at about the 50th sample after the onset of the change (that is, after five time constants). In contrast, using SSPCA, the NOC limits are $3 \cdot \sqrt{s} \cdot \sigma$, with the nominal steady-state location of the shifted data extending to $3 \cdot s \cdot \sigma$. This increased resolution between the NOC and the failure point will often lead to a faster identification of the

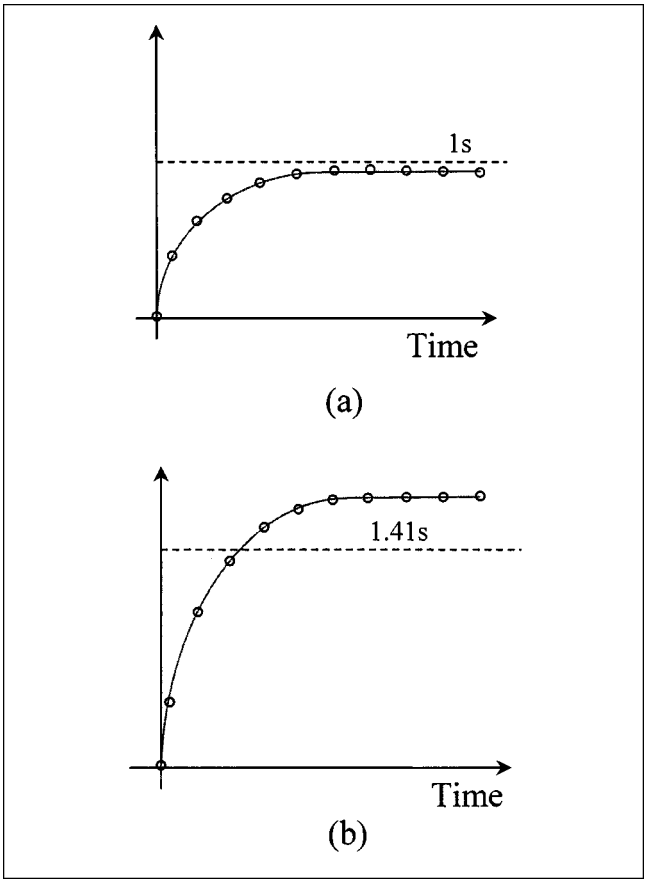

Figure 2. Dynamics of nominal shift behavior for (a) conventional PCA, and (b) summed-scores PCA, with $s = 2$.

alarm status. Thus, returning to the same disturbance as before, SSPCA with $s = 2$ detects an alarm at the 14th sample, as shown in Figure 2. In the following, the term ''outlier'' refers to measured data that fall outside normal operating limits.

Since the increase in resolution afforded by SSPCA over conventional PCA is by a factor of $\sqrt{s}$ for the ideal case, it will increase with s, although at the price of delayed reaction. Thus, the appropriate selection of the value of s depends on the sensitivity to disturbances that is required from the monitoring system. For gross alarm detection, when the disturbance or failure is of sufficient magnitude to drive the scores well outside the NOC limits, conventional PCA may suffice to give adequate performance. On the other hand, it may be of interest to detect constant shifts within what is considered to be normal behavior, which can be accomplished with the SSPCA approach by selecting the value of s appropriately. The so-called accumulated-scores PCA (ASPCA), suggested by Zhang et al. (1996), is equivalent to SSPCA with $s \to \infty$. The implementation of ASPCA leads to two main disadvantages. First, it generates NOC data that are not normally distributed, and usually with a nonzero mean, which may lead to interpretation problems. A second, more serious disadvantage is its sluggish performance in dealing with transient data, a consequence of setting $s \to \infty$.

Another side benefit achieved by applying the suggested method is that by moving the clusters of shifted fault-data further away from NOC boundaries, the view angle as projected back from the outlier cluster is reduced, allowing for a more accurate mapping of faults, which improves the identification performance, as shown in Figure 3. This enhanced resolution is reflected by the view-angle ratio, R_θ, which can be easily derived by trigonometry as

$$R_\theta = \frac{\theta}{\hat{\theta}} = \frac{\tan^{-1}\left(\frac{\sigma}{\delta}\right)}{\tan^{-1}\left(\frac{\sigma}{\delta \cdot \sqrt{s}}\right)}, \tag{12}$$

where δ is the shift size. This ratio increases with increasing s, limiting by the asymptotes: $R_\theta \to \sqrt{s}$ for $\sigma/\delta \ll 1$, and $R_\theta \to 1$ for $\sigma/\delta \gg 1$.

The motivation for the improvements described in this article is to increase the disturbance and failure resolution afforded by PCA. Several measures will be used, relating to disturbance isolation and resolution, and these are defined next.

Multidimensional NOC volume, V_{NOC}

A measure of the resolution afforded by PCA is the volume spanned by what is considered to be NOC in the multidimensional scores plane, V_{NOC}, which can be computed either as the product of the principal component standard deviations, or equivalently, as the product of the roots of the correlation matrix eigenvalues:

$$V_{NOC} = \prod_{i=1}^{m} 3\sigma_i(A) = \prod_{i=1}^{m} 3\sqrt{\lambda_i(A)}\,. \tag{13}$$

Note that the factor of 3 in Eq. 13 enters as a result of the 3σ limits previously mentioned. Since a useful property of the correlation matrix is that its determinant equals the product of its eigenvalues,

$$V_{NOC} = 3^m \prod_{i=1}^{m} \sqrt{\lambda_i(A)} = 3^m \sqrt{|A|}\,, \tag{14}$$

increased resolution through a reduction in V_{NOC} is equivalent to minimizing the determinant of the correlation matrix.

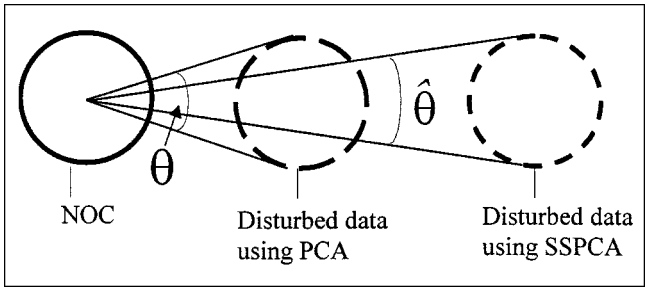

Figure 3. Potential departure angles for shifted data obtained using conventional PCA and SSPCA on a plane of two principal components.

Euclidean distance to failure, r

The Euclidean distance to failure is the mean distance between the origin and the location of the failure/disturbance in the normalized scores plane. Normalization of the scores plane is by division of each score coordinate by the root of the corresponding eigenvalue:

$$r = \sqrt{\sum_{i=1}^{m} \frac{\left(T_i^D\right)^2}{\lambda_i}}, \tag{15}$$

where T_i^D is the average value of the ith PC scores at the failure location.

Isolation ratio, I

The isolation ratio is the ratio between the Euclidean distance to failure and the distance from the origin to the NOC limits, which can be expressed as

$$I = \frac{r}{3\sqrt{m}}. \tag{16}$$

Enhanced disturbance resolution is achieved by increasing the distance between NOC data and shifted data. The SSPCA approach succeeds in doing this by shifting disturbed data from the origin by a factor of $\sqrt{s}$ more than its shift in NOC data. An alternative is to produce a "tighter" NOC model, through contraction of V_{NOC}. This is carried out by improving the correlation between the process variables in transient data by considering the dynamics or delays present between them. This is discussed next.

Delay-Adjusted PCA

In delay-adjusted PCA (DAPCA), the data are preprocessed, applying relative shifts between the inputs and outputs. The optimal shifts in each input variable are those that minimize the determinant of the associated correlation matrix. The algorithm is

1. Form the $n \times m$ raw data matrix, X, consisting of n rows (n observations) and m columns (m variables), the first k of which are inputs and the subsequent $m - k$ are outputs: $X = [x_1, \ldots, x_k, x_{k+1}, \ldots, x_m]$.
2. Define the maximum reasonable process delay, d_{max}, in terms of samples.
3. For each input variable, i: (a) form the $n \times (m - k + 1)$ data matrix, X_i, from the ith input and all $m - k$ outputs; (b) select the optimal backward shift in the ith input, d_i, in the range $0 \le d_i \le d_{\max}$, such that the derminant of the correlation matrix computed from X_i is minimized. The search for d_i is carried out by enumeration; (c) store the optimal shift for the ith input, d_i.
4. Adjust the original data set such that each input vector is shifted by its optimal delay, $Y = [x_{1,d_1}, \ldots, x_{k,d_k}, x_{k+1}, \ldots, x_m]$; and
5. Perform PCA on the modified data set, and adjust new samples by the optimal shifts computed in step 3.

The algorithm assumes that the output variables are correlated among themselves with no delays present, and that the inputs are independent of each other. This may not always be true, especially when analyzing closed-loop data. Thus, since only correlations between the outputs and inputs are optimized, it is not possible to guarantee that the proposed algorithm always identifies the optimal shifts that find the global minimum for V_{NOC}. An alternative algorithm could be applied, requiring an exhaustive search over all combinations between the m variables. However, since such an algorithm requires as much as $(d_{\max})^m$ computations of the determinant of the correlation matrix, its implementation is infeasible in processes with a large number of variables. In contrast, the proposed algorithm requires up to $d_{\max} \times k \times (m - k)$ calculations of the determinant of the correlation matrix, where k is the number of inputs. The use of the DAPCA algorithm is now illustrated on two examples.

Example 2. Consider the example used by Kramer (1991) to demonstrate nonlinear PCA:

$$u = 0.8 \cdot \sin\theta \tag{17a}$$

$$y = 0.8 \cdot \cos\theta \tag{17b}$$

$$\theta = W[0, 2\pi], \tag{17c}$$

where $W[a, b]$ represents the uniform distribution in the range (a, b). A data set, comprising of 100 samples, is collected and stored in the matrix, $X = [u, y]$. Performing PCA on the raw data produces the orthogonal eigenvectors: $p_1 = [\sqrt{0.5} \ \sqrt{0.5}]^T$ and $p_2 = [\sqrt{0.5} \ -\sqrt{0.5}]^T$ with corresponding eigenvalues $\lambda_1 = 1$ and $\lambda_2 = 1$. This implies that there is no correlation between the two variables and that both directions describe the same amount of variability in the data. Using DAPCA, it is found that by delaying the input variable, u, relative to the output variable, y, by 25 samples (corresponding to 0.5π), the determinant of the correlation matrix is 0, and so V_{NOC} is reduced to zero. Performing PCA on the modified array will produce eigenvalues $\lambda_1 = 2$ and $\lambda_2 = 0$ associated with the same eigenvectors as before. Using the known shift for further analysis will allow the use of one principal component to model the normal data with no loss of information.

Example 3. Wood and Berry (1973) present a linear model approximating the dynamics of a binary distillation column separating methanol from water, in which the distillate and bottoms methanol weight fraction are expressed as functions of reflux and reboiler steam flow rates. Their continuous model, sampled at a time interval of one minute, gives the difference equations:

$$X_{D,i} = 1.895 X_{D,i-1} - 0.898 X_{D,i-2} + 0.744 R_{i-2} - 0.709 R_{i-3} - 0.879 S_{i-4} + 0.828 S_{i-5} \tag{18a}$$

$$X_{B,i} = 1.845 X_{B,i-1} - 0.851 X_{B,i-2} + 0.579 R_{i-8} - 0.54 R_{i-9} - 1.302 S_{i-4} + 1.187 S_{i-5}. \tag{18b}$$

In Eqs. 18, X_B and X_D are the percentage methanol weight fractions in the distillate and bottoms product, and R and S are the reflux and reboiler steam flow rates, with all variables expressed as deviations from their nominal steady-state values. Normal behavior is simulated by generating 1,000

Table 1. Correlation Matrix Eigenvalues for the Raw and Shifted Data Sets

	λ_1	λ_2	λ_3	λ_4	V_{NOC}
X	1.91	1.01	0.99	0.10	**35.3**
X_{DA}	2.08	1.02	0.83	0.08	**29.2**

samples of data in which R and S are normally distributed vectors having mean zero and unit variance, and X_B and X_D are computed according to Eqs. 18 with the addition of measurement noise (assuming normally distributed noise with zero mean and 0.01 standard deviation). The application of the delay-adjustment algorithm to the generated data indicates that the optimal backward shifts in the input vectors R and S are two and four samples, respectively. Eigenvalues of the correlation matrix obtained for the raw array and the modified one are given in Table 1.

To investigate the impact of the preceding results, various faults and disturbances were simulated, and the resolution capabilities of PCA using the original and the DA-modified data sets were compared. The two process disturbances simulated were constant shifts in R and S, one at a time, and four sensor faults were simulated as constant shifts in the values of each variable, one at a time. Each disturbance or fault set consisted of 1000 samples in each run. The results of the tests are presented in Table 2. Clearly, there is no marked improvement in the process disturbance resolution afforded by DAPCA, whereas for sensor fault detection, the improvement is statistically significant (up to 14% better). These results can be elucidated by first noting that the DA-modification actually *increases* the normal operation variability range, as reflected by the higher value of the first eigenvalue, while *decreasing* the permitted operation range in scores capturing the allowed variation in the physical relations between the variables (as captured in the last two eigenvalues). Next, we note that disturbances will manifest themselves as possibly increasing the observed operating range, whereas sensor faults cause violations in the necessary physical relations between the variables. Thus, the increased ''tightness'' of the model so obtained explains why mismatches in the allowed interrelation between the variables are trapped more effectively. This is shown in the two-dimensional example in Figure 4.

Algorithm for Failure and Disturbance Identification

The algorithm involves off-line data manipulation, delay-adjustment, PCA model-building and NOC definition steps. Once the NOC is defined in the principal component (PC) space, on-line failure diagnosis can be implemented. These steps are described in detail next.

Table 2. Mean Shift of Applied Faults and Disturbances

	$r \pm \sigma(r)$	$r_{DA} \pm \sigma(r_{DA})$
Shift in R	4.46 ± 0.21	4.41 ± 0.21
Shift in S	5.79 ± 0.20	5.71 ± 0.20
Fault in R	2.02 ± 0.02	2.30 ± 0.02
Fault in S	2.04 ± 0.03	2.23 ± 0.03
Fault in X_B	2.36 ± 0.10	2.64 ± 0.10
Fault in X_D	2.45 ± 0.13	2.76 ± 0.14

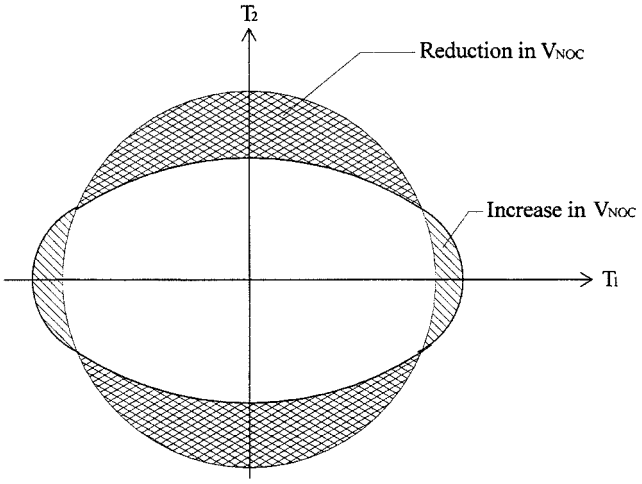

Figure 4. Two-dimensional example showing tighter model obtained with DAPCA.

Data Manipulation. The process measurements representing normal operating conditions are stored in a matrix X with n (observations) rows and m (sensors) columns. The data are usually autoscaled; that is, the entries in each column are subtracted by their mean values and divided by their standard deviations.

Delay Adjustment. The optimal backward shift is determined for each input variable, using the algorithm presented in the third section. The resulting data are stored in a matrix Y. In some cases, and particularly when analyzing closed-loop data, this step may be omitted, and Y taken as X.

Off-Line Modeling Using PCA. The $m \times m$ correlation matrix is formed using Y:

$$A = \frac{Y^T Y}{n-1}. \tag{19}$$

The eigenvectors and eigenvalues of A are computed and arranged by decreasing order of eigenvalue magnitudes. The scores on the new coordinate system are computed: $T = PY$. A reduced-order model is defined, using the first k loadings, deemed sufficient to capture most of the data variance (using cross-validation, SCREE plot, arbitrarily defined percentage variability capture, or other techniques. See Jackson (1989) for more details).

$$Y_m = t_1 p_1^T + t_2 p_2^T + \cdots + t_k p_k^T + \cdots + t_m p_m^T \tag{20}$$

$$Y = Y_m + R. \tag{21}$$

Finally, the summed-scores construct is calculated for the scores:

$$\tilde{t}_k = t_k + t_{k-1} + \cdots + t_{k-s}. \tag{22}$$

Computing the NOC Envelope. The NOC limits should be defined for each process specifically, according to which type

of error is more important. For example, if one operates a potentially unsafe process, it is clearly preferable to receive false alarms rather than not to receive an alarm when a real shift has occurred (that is, Type I and Type II error considerations should be accounted for). As a general rule, though, it will be assumed that one seeks to minimize false alarms and the limits will be defined as three times the standard deviation of the $\tilde{t}$ vectors, ensuring that 99.74% of normal distributed data in normal conditions are inside the NOC boundary limits. Thus, if only the first two principal components are used, the NOC boundaries will be elliptical, with principal radii $3\sigma(\tilde{t}_1)$, $3\sigma(\tilde{t}_2)$, respectively. If data of higher dimension must be maintained, a general measure such as Hotelling's T^2 should be used. Residual analysis is carried out with the Q-statistic:

$$Q = (Y - Y_m)^T (Y - Y_m), \tag{23}$$

with the statistical limit,

$$Q_\alpha = \theta_1 \left[\frac{c_\alpha \sqrt{2\theta_2 h_0^2}}{\theta_1} + \frac{\theta_2 h_0 (h_0 - 1)}{\theta_1^2} + 1 \right]^{1/h_0}, \tag{24}$$

where

$$\theta_1 = \sum_{i=k+1}^{m} \lambda_i, \qquad \theta_2 = \sum_{i=k+1}^{m} \lambda^2, \qquad \theta_3 = \sum_{i=k+1}^{m} \lambda^3,$$

$$\text{and} \qquad h_0 = 1 - \frac{2\theta_1\theta_3}{\theta_2^2}.$$

In the preceding, λ_i is the ith eigenvalue of the correlation matrix and c_α is the normal deviate cutting off an area of α under the upper tail of the distribution, with its sign equal to the sign of h_0.

Mapping the Disturbances. If two or three principal components are sufficient to describe the data with an adequate resolution, mapping departure directions from NOC boundaries can be carried out on the scores plane for known disturbances, in conjunction with residual analysis. Mapping of higher dimensions, or even projection of all of the principal components simultaneously, may be obtained using parallel coordinates (Wachs et al., 1999).

On-Line Process Monitoring. New data are monitored against the NOC and its alarm limits. Each new observation vector is autoscaled and projected onto the principal component space. The modified sample vector is then summed with the preceding $s-1$ score vectors to form the summed-scores data vector. An alarm for a shift in the process occurs when the values of $\tilde{T}$ move out of the defined NOC envelope. When such an alarm occurs, the departure direction should be compared to the disturbance map for identification. After certain identification, its data should be added to the mapping data, so its accuracy will improve with time (Lewin, 1995).

In the following, disturbance diagnosis and identification using the SSPCA algorithm is demonstrated on two industrially relevant case studies: an exothermic CSTR and the Tennessee Eastman process simulation.

Case Study 1: Disturbance Diagnosis for a CSTR

Allgöwer and Ilchmann (1995) provide a model that describes several reactions taking place in a CSTR: (1) $A \rightarrow B$, (2) $B \rightarrow P$, and (3) $B \rightarrow X$, in which A is the raw material, and B, P, and X are the intermediate, desired, and undesired reaction products. Reactions (1) and (2) are exothermic, reaction (3) is endothermic, and since the overall reaction is exothermic, the reactor is equipped with a cooling jacket to allow temperature control.

Modeling. The process is described in terms of its state variables $x = (C_A, C_B, C_P, T, T_j)$, manipulated variables $u = (q, q_j)$, and outputs $y = (C_P, T, T_j, q, q_j)$, in which T and T_j are the reactor and cooling jacket temperatures; C_A, C_B, and C_P are the concentrations of A, B, and P; and q and q_j are the reactor feed flow and cooling water flow rates. The reactor is modeled by the differential equations:

$$\dot{C}_A = q(C_{A0} - C_A) - k_1(T) \cdot C_A \tag{25}$$

$$\dot{C}_B = -qC_B + k_1(T) \cdot C_A - k_2(T) \cdot C_B - k_3(T) \cdot C_B \tag{26}$$

$$\dot{C}_P = -qC_P + k_2(T) \cdot C_B \tag{27}$$

$$\dot{T} = q(T_0 - T) - \frac{1}{\rho p} \cdot \left[k_1(T) \cdot C_A \cdot \Delta H_1 + k_2(T) \cdot C_B \cdot \Delta H_2 + k_3(T) \cdot C_B \cdot \Delta H_3 \right] + \cdots - \frac{U \cdot A}{V \cdot \rho p} \cdot (T - T_j) \tag{28}$$

$$\dot{T}_J = q_j(T_{j0} - T_j) + \frac{U \cdot A}{V_j \cdot \rho p} \cdot (T - T_j). \tag{29}$$

The reaction rates follow Arrhenius relationships:

$$k_i(T) = k_{i0} \cdot \exp\left\{ \frac{E_i}{T} \right\} \qquad i = 1, 2, 3. \tag{30}$$

The physical properties, together with the values of the process variables at the operating-point steady state, are summarized in Table 3.

Control. A control scheme was implemented to regulate T and C_P, by manipulating q and q_j. A decentralized PID control scheme was designed, with the controller pairings selected using the dynamic RGA, with the loops being $T - q$ and $C_P - q_j$. Finally, the controllers were tuned using the IMC-PID rules (Rivera et al., 1986). This model-based scheme

Table 3. Physical Parameters and Process Variable Values at Steady State

Variable		Value	Variable		Value
C_P	[M][M]	1.00	k_{10}	[min^{-1}]	1.169×10^{10}
T	[K]	353.15	k_{20}	[min^{-1}]	1.445×10^{11}
q	[min^{-1}]	0.15	k_{30}	[min^{-1}]	1.689×10^{11}
q_j	[min^{-1}]	0.10	E_1	[K]	9,000
$C_{A,0}$	[M][M]	5.00	E_2	[K]	9,500
T_0	[K]	343.15	E_3	[K]	9,800
T_{j0}	[K]	288.15	ΔH_1	[kJ/mol]	-40
UA/V	[1 K/kJ·min]	0.225	ΔH_2	[kJ/mol]	-20
ρC_p	[kJ/K]	1.00	ΔH_3	[kJ/mol]	120

relied on the process model, linearized in the vicinity of the operating point, with the tunings ensuring that each individual control loop satisfied robust stability and that the whole system guarantees closed-loop stability despite process interactions. The following controllers were obtained:

$$\text{Loop 1: } C_1(s) = \frac{4.05\times10^{-4}\cdot(2s+1)(10s+1)}{s(1.4s+1)} \tag{31}$$

$$\text{Loop 2: } C_2(s) = \frac{-8.3\times10^{-3}\cdot(8s+1)^2}{s(1.5s+1)}. \tag{32}$$

Five variables were assumed to be continuously available, namely C_P, T, T_j, q, and q_j, while the disturbances to be diagnosed were abnormally high step changes in C_{A0}, the feed concentration, T_0, the feed temperature, T_{j0}, the cooling water inlet temperature, and a slow accumulation of fouling as modeled by a gradually decreasing heat-transfer coefficient, U. Modest changes in the first three disturbance variables were considered normal, namely ±0.3 M in C_{A0}, and ±3°C and ±5°C in T_0 and T_{j0}, respectively. The control system implemented attenuates the effect of these levels of disturbances and maintains C_P and T within ±0.02 M and ±1°C of their setpoints (assuming measurement noise to be insignificant).

Applying the Method. A simulation was carried out over 4,000 min, with normal disturbance variations occurring randomly, with the data for NOC sampled at 5-min intervals. The NOC envelope, computed following the algebraic steps described earlier, but without implementing delay adjustment, was defined in two-dimensional scores space, following the observation that about 95% of the data variability is captured by the first two principal components.

Disturbance Diagnosis. Each of the four disturbances mentioned earlier was applied to the system with random step sizes of predefined ranges, and at a random time of occurrence. The effect of each disturbance was simulated 200 times, with perturbations imposed in both positive and negative directions relative to the nominal value. Two ranges of disturbance sizes were examined, one with shifts smaller than normal, and in that case $s = 10$ was selected for SSPCA, and the second with disturbance magnitudes of between twice and three times the normal values, for which $s = 4$ was found to

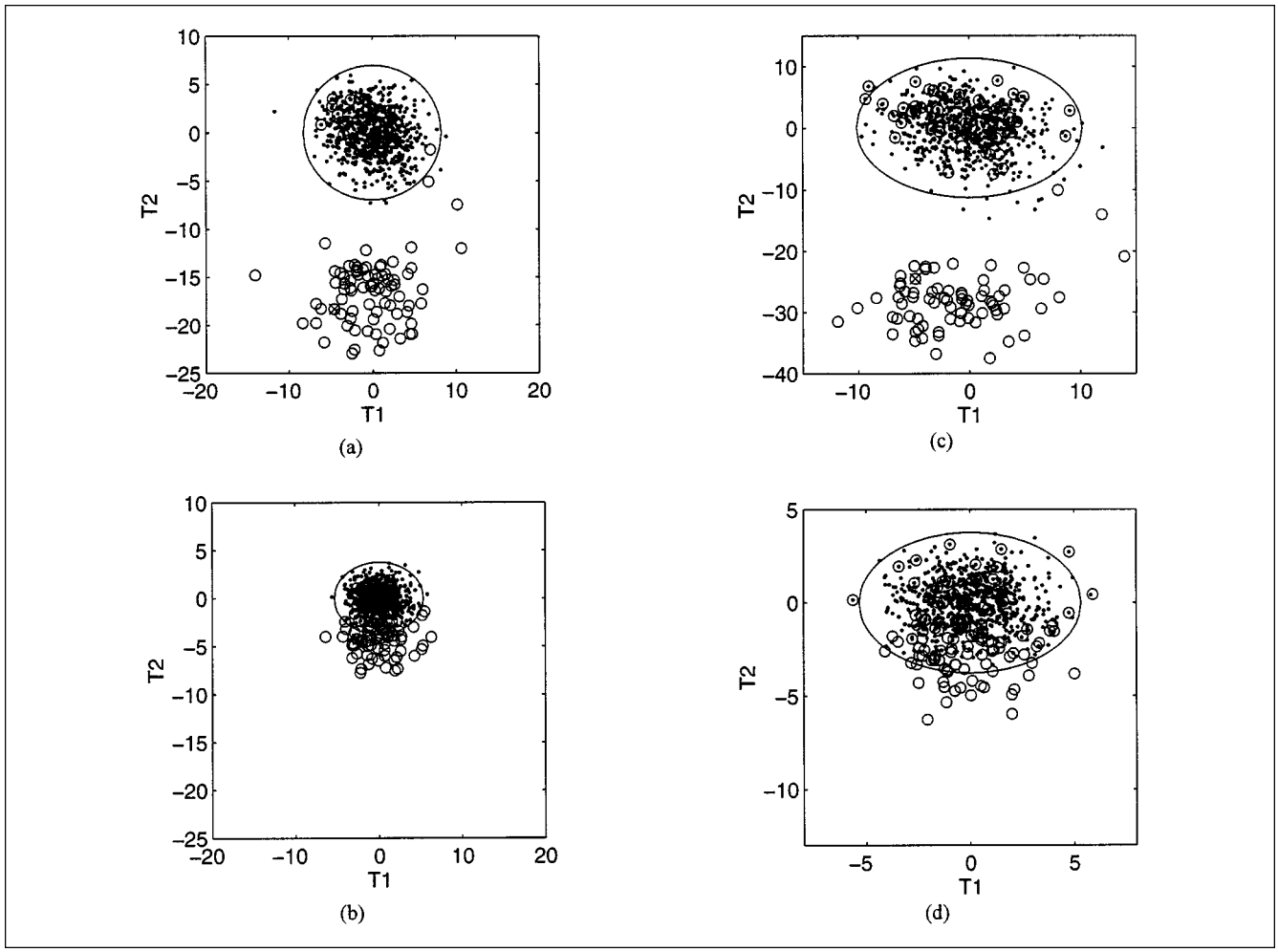

Figure 5. Disturbance diagnosis with PCA and SSPCA.

Normal data are shown by dots, while disturbed data by circles: (a) SSPCA, large shift, $s = 4$; (b) PCA, large shifts; (c) SSPCA, small shift, $s = 10$; (d) PCA, small shifts.

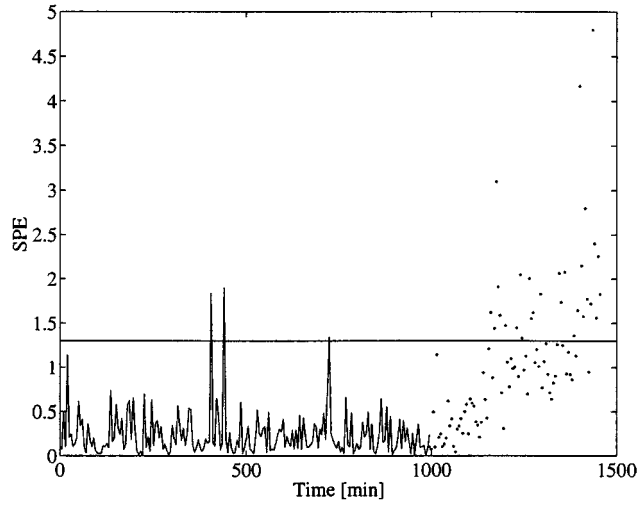

Figure 6. Residual analysis for a shift of +0.1 in CaO: (a) raw data; (b) summed scores, $s = 10$.

provide good performance. For each case, the elapsed number of samples, t_0, from the instant that the disturbance occurs until the NOC limits were crossed were recorded, as were the directions in which the *T*-vector crossed the NOC envelope (θ_0), and that of the last sample (θ_f), at 400 minutes, which was taken as the steady-state disturbance direction. These results were compared with the performance of conventional PCA on the raw measurements with the same disturbances, as illustrated in Figure 5, where resolution enhancement with SSPCA between normal and disturbed data for both large and small shifts in disturbances is noted. Residual analysis indicates that all disturbances showed deviations on the residual plane with both PCA and SSPCA, although the latter provides sharper transitions between the NOC and alarm conditions, as shown by the example in Figure 6.

The results for large and small disturbances are summarized in Tables 4 and 5, respectively. It can be seen that the number of samples between occurrence and diagnosis, t_0, is much smaller than the number of samples for each run (81), so the assumption of steady state is reasonable.

Although the average value of t_0 is similar for both PCA and SSPCA, a significant reduction in departure-angle range is obtained using SSPCA, as reflected by the smaller values of the standard deviation statistic, $\sigma(\theta_0)$, so obtained. Figure 7 shows pie-chart representations of the steady-state scores-plane directions obtained by the two methods, for the two levels of disturbance magnitude tested. In each figure, the effect of each disturbance is projected as a sector in the pie chart whose limits are delineated according to $\bar{\theta}_f \pm \sigma(\theta_f)$. It is noted that the sectors representing the projections for the final directions for SSPCA are distinct and do not overlap. This means that, for the disturbances investigated, the cause of every outlier that falls into one of the known departure-angle ranges can be uniquely identified. Furthermore, the results obtained using SSPCA appear to be independent of the disturbance magnitude tested. All of this is in marked contrast with the results obtained with conventional PCA, where there is significant overlapping, meaning that identification of the cause of most of the outliers would be ambiguous. An additional advantage of SSPCA over PCA is the improvement of the *isolation ratio, I*. For $s = 4$ and 10, the values of I for SSPCA were about 2.5 and 3.8 times larger than for PCA, which fits the analytical expectations of increased ability to isolate disturbances with increasing s.

Case Study 2: Disturbance Diagnosis for the Tennessee Eastman Process

SSPCA was applied to the diagnosis of disturbances for the Tennessee Eastman industrial process simulation, introduced by Downs and Vogel (1993). In this process, two products, *G* and *H*, as well as one unwanted byproduct, are produced from four feed streams consisting of four reactants: *A*, *C*, *D*,

Table 4. Detection Performance of PCA and SSPCA (Large Disturbances)

		Conventional PCA					SSPCA				
Dist.	Range	$\bar{t}_0$	$\bar{\theta}_0$	$\sigma(\theta_0)$	$\bar{\theta}_f$	$\sigma(\theta_f)$	$\bar{t}_0$	$\bar{\theta}_0$	$\sigma(\theta_0)$	$\bar{\theta}_f$	$\sigma(\theta_f)$
$C_{A,0}$	$-0.3 \Leftrightarrow 0.5$	4	351°	21	292°	19	5	340°	14	271°	9
	$0.3 \Leftrightarrow 0.5$	4	127°	36	62°	10	5	136°	21	77°	6
T_0	$-3 \Leftrightarrow -5$	4	357°	16	321°	13	4	352°	12	297°	10
	$3 \Leftrightarrow 5$	3	151°	31	74°	16	4	157°	15	97°	8
T_{j0}	$5 \Leftrightarrow 8$	5	15°	17	3°	17	5	25°	12	348°	21
U	$0.225 \Rightarrow 0$	10	355°	21	290°	3	10	322°	23	285°	2

Table 5. Detection Performance of PCA and SSPCA (Small Disturbances)

		Conventional PCA					SSPCA				
Dist.	Range	$\bar{t}_0$	$\bar{\theta}_0$	$\sigma(\theta_0)$	$\bar{\theta}_f$	$\sigma(\theta_f)$	$\bar{t}_0$	$\bar{\theta}_0$	$\sigma(\theta_0)$	$\bar{\theta}_f$	$\sigma(\theta_f)$
C_{A0}	$-0.1 \Leftrightarrow -0.3$	6	347°	20	318°	32	8	332°	18	268°	8
	$0.1 \Leftrightarrow 0.3$	7	77°	50	49°	17	7	121°	22	80°	6
T_0	$-1 \Leftrightarrow -3$	7	353°	16	340°	23	7	349°	13	294°	10
	$1 \Leftrightarrow 3$	11	95°	60	57°	26	7	140°	17	102°	9
T_{j0}	$2 \Leftrightarrow 5$	12	6°	16	10°	24	8	23°	11	346°	26
U	$0.225 \Rightarrow 0$	10	355°	21	290°	3	13	323°	18	284°	1

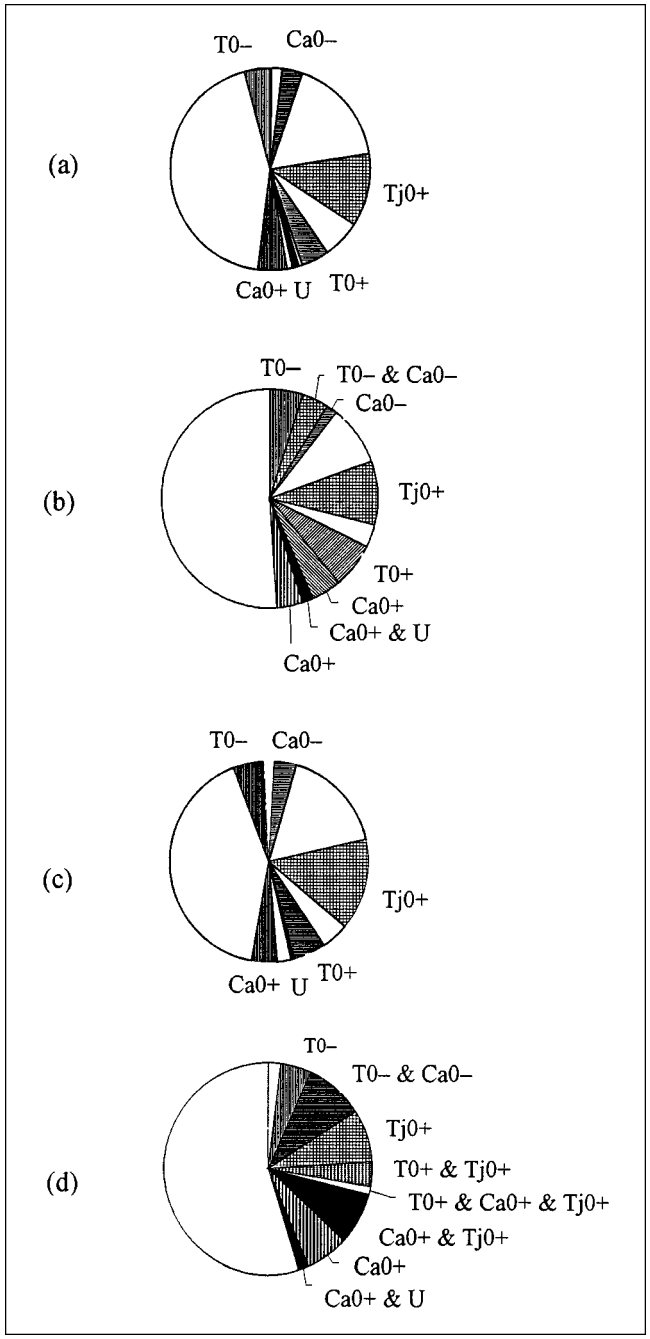

Figure 7. Steady-state disturbance direction mapping for CSTR failure identification.

(a) SSPCA, large shift, $s = 4$; (b) PCA, large shifts; (c) SSPCA, small shift, $s = 10$; (d) PCA, small shifts.

and E, and an inert component, B. The main process units in the flow sheet are a reactor, separator, stripper, condenser, and a compressor, and the system involves 12 manipulated variables and 41 process measurements of which 22 are continuous and the rest measure concentrations at intervals of 6 or 15 min. The logged process variables, organized into groups associated with the reactor, stripper, and separator for the purposes of decentralized diagnosis, are shown in Figure 8, which also indicates the sources of the first seven disturbances that are to be identified, noting that the disturbances are numbered as they appear in the original article.

There has been significant activity in the application of disturbance diagnosis methods to this problem (such as Ku et al., 1995; Georgakis et al., 1996; Raich and Cinar, 1996, 1997; Wachs and Lewin, 1998). However, comparison between the reported results is difficult, since each study employs a different control scheme, which affects the system behavior and the consequent correlation between the process variables. Moreover, none of the reported studies have simulated varying disturbance magnitudes, and therefore lack generality, since then, each disturbance is defined strictly by its magnitude.

In this study, the process was controlled using the configuration proposed by McAvoy and Ye (1994), which utilizes the first 11 manipulated variables. Data describing normal operating conditions were collected from 40 h of simulated operation of the process. It should be noted that only the 22

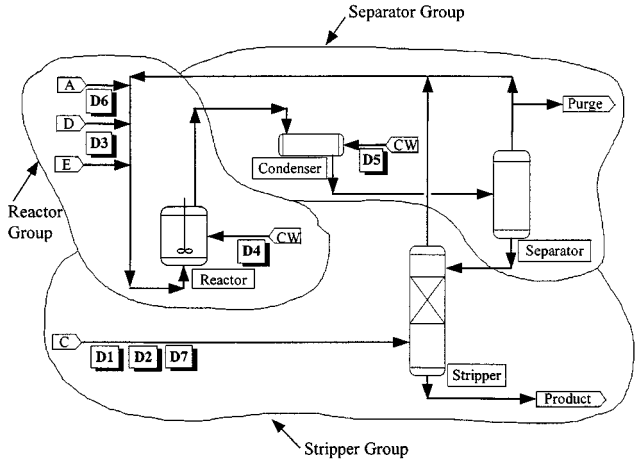

Figure 8. Tennessee Eastman Process, showing the three diagnosis groups and the disturbance sources.

continuous output measurements and the 11 manipulated variables were used for diagnosis, sampled at 3-min intervals, thus the sparser composition measurements were not used. The main reason for neglecting these was to avoid the consequences of interpolation on the diagnosis procedure. The sample interval affects the degree of correlation in the system and is usually selected to be an order of magnitude smaller than the dominant characteristic time of the process. The value selected was that used by Georgakis et al. (1996), allowing a comparison with their results. The 33 measurements were divided between three diagnosis groups, associated with the reactor, separator, and stripper, following the decentralized approach suggested by Georgakis et al. (1996). As a result, the dimensionality of the data that needs to be dealt with in each group is significantly less than that of the complete data set, thus increasing the likelihood of being able to isolate the disturbances. Furthermore, the decentralization of the diagnosis has the additional advantage of being able to pinpoint the source of the disturbance by identifying which group violates its NOC limits first.

The performance of conventional PCA on the Tennessee Eastman problem is rather disappointing, with many disturbances not uniquely identified. However, the diagnosis performance is significantly improved when employing decentralized SSPCA with $s = 5$. The rather arbitrary selection of s reflects the desired sensitivity and on how much diagnosis delay is acceptable. It was found that three principal components could explain 90% of the data variability for each group (that is, a total of nine were used). Thus, a three-dimensional presentation on the scores-plane is implemented, with two solid angles describing the direction of an outlier for each unit when it occurs. By adapting the original simulation-code, disturbances of known types with varying magnitudes were imposed on the simulated process. This modification is of importance when testing fault diagnosis strategies, since the scores trajectories change with disturbance size, and algorithms that use a "disturbance bank" with one profile fitted to each kind of disturbance, (such as Raich and Cinar, 1996; Ku et al., 1995) are not general enough to deal with disturbances of varying sizes. Each disturbance was simulated 100 times with varying time of occurrence and magnitude (within a prespecified range). For each instance, the solid angles of departure from NOC (θ, φ) for each group and the sequence and intervals between departures of the different NOC groups were recorded, as shown in Table 6. The number of samples between the registered alarms are not included in the mapping, since they show low specificity and do not add valuable information. The departing order entries have values of either 1 or 0, denoting whether a certain unit was observed to depart from its NOC limits in the specified order. It can be seen that the definitions are rather unique, and even though there is some overlap, no disturbance registration is identical to another. Thus, for example, Disturbance 1 (with a positive direction) departs either first or second from the reactor NOC group (with average solid angles of $\theta = 308°$ and $\varphi = 74°$, as shown in the first row in Table 6a), either second or first from the stripper NOC group (with average solid angles of $\theta = 13°$ and $\varphi = 62°$, as shown in the first row in Table 6c), and last from the separator NOC group (with average solid angles of $\theta = 186°$ and $\varphi = 92°$, as shown in the first row in Table 6b).

Table 6. Mapping Disturbance Departures from NOC Group

Disturbance Number	Disturbance Range	Departing Order			θ Range		φ Range	
		1	2	3	$\mu(\theta)$	$\sigma(\theta)$	$\mu(\varphi)$	$\sigma(\varphi)$
(a) *Reactor*								
1	$0.4 \Leftrightarrow 1.6$	1	1	0	308	14	74	8
	$-0.4 \Leftrightarrow -1.6$	1	1	0	131	14	107	6
2	$0.4 \Leftrightarrow 1.6$	1	0	0	307	12	68	9
	$-0.4 \Leftrightarrow -1.6$	1	0	0	126	17	112	7
3	$2 \Leftrightarrow 5$	1	1	0	23	9	94	6
	$-2 \Leftrightarrow -5$	1	1	0	189	8	88	5
4	$0.4 \Leftrightarrow 1.6$	1	0	0	58	12	101	9
	$-0.4 \Leftrightarrow -1.6$	1	0	0	224	11	83	8
6	$0.1 \Leftrightarrow 0.8$	1	0	0	339	7	59	6
	$-0.1 \Leftrightarrow -0.8$	1	0	0	151	13	121	9
7	$0.4 \Leftrightarrow 1.6$	1	1	0	168	8	109	4
	$-0.4 \Leftrightarrow -1.6$	1	1	0	348	5	70	4
(b) *Separator*								
1	$0.4 \Leftrightarrow 1.6$	0	0	1	186	6	92	3
	$-0.4 \Leftrightarrow -1.6$	0	0	1	354	6	79	4
2	$0.4 \Leftrightarrow 1.6$	0	1	1	178	7	79	5
	$-0.4 \Leftrightarrow -1.6$	0	1	1	349	5	92	4
3	$2 \Leftrightarrow 5$	1	1	0	292	6	100	7
	$-2 \Leftrightarrow -5$	1	1	0	114	59	77	8
4	$0.4 \Leftrightarrow 1.6$	—	—	—	—	—	—	—
	$-0.4 \Leftrightarrow -1.6$	—	—	—	—	—	—	—
6	$0.1 \Leftrightarrow 0.8$	—	—	—	—	—	—	—
	$-0.1 \Leftrightarrow -0.8$	—	—	—	—	—	—	—
7	$0.4 \Leftrightarrow 1.6$	1	1	0	78	5	103	4
	$-0.4 \Leftrightarrow -1.6$	1	1	0	260	6	76	4
(c) *Stripper*								
1	$0.4 \Leftrightarrow 1.6$	1	1	0	13	12	62	10
	$-0.4 \Leftrightarrow -1.6$	1	1	0	217	12	110	6
2	$0.4 \Leftrightarrow 1.6$	0	1	1	282	51	29	10
	$-0.4 \Leftrightarrow -1.6$	0	1	1	315	31	141	12
3	$2 \Leftrightarrow 5$	—	—	—	—	—	—	—
	$-2 \Leftrightarrow -5$	—	—	—	—	—	—	—
4	$0.4 \Leftrightarrow 1.6$	—	—	—	—	—	—	—
	$-0.4 \Leftrightarrow -1.6$	—	—	—	—	—	—	—
6	$0.1 \Leftrightarrow 0.8$	—	—	—	—	—	—	—
	$-0.1 \Leftrightarrow -0.8$	—	—	—	—	—	—	—
7	$0.4 \Leftrightarrow 1.6$	0	1	1	303	32	139	14
	$-0.4 \Leftrightarrow -1.6$	0	1	1	156	18	33	21

The first seven disturbances refer to step changes in concentrations, temperatures, and flows. As shown in the tables, disturbances with opposite signs cross the NOC boundaries at approximately opposite sides of the NOC envelope. Clearly, disturbances defined as random variations cannot be mapped using this approach. Several disturbances do not register departure from NOC in all three groups, namely Disturbance 3, which does not affect the stripper group, and Disturbances 4 and 6, which only affect the reactor group.

On examination of the residual data, it was found that all of the disturbances that violate the NOC limits also crossed the normal level of residual deviation, and therefore analysis of residuals does not add any additional discriminating information. The only exception was Disturbance 5, which did not show deviation on the scores plane, but moved out of the normal residual level for the separator group. The disturbance resolution is enhanced by increasing s: for the values $s = 2$, 5, and 20, the ratio of the mean residual value with and without applying SSPCA were approximately 1.1, 1.4, and 3.5, respectively.

On-line detection

An on-line detection procedure was programmed to keep track of how the effect of a detected disturbance matches up against each known disturbance's mapping registration. The following algorithm detects and identifies a disturbance:

1. *Projection of the New Sample's Data into the Three Groups' Scores-Plane*.

2. *Detection of Outlier*. In principle, an alarm is triggered as soon as the NOC limits of one of the diagnosis groups is violated. This makes the algorithm rather sensitive and potentially prone to register false alarms; modifications to reduce sensitivity should be considered.

3. *Computation of a Matching Coefficient Against Each Known Disturbance*. The disturbance mapping, available for each known disturbance, is used to assign feasibility cause to the observed situation. Each time new information is logged, a matching coefficient, M, is computed:

$$M = \sqrt[i]{\prod_i p_i}, \tag{33}$$

where p_i is the probability density function for a given match of each solid departure-angle for the relevant diagnosis group:

$$p_i = \int_{\theta_i}^{\infty} \frac{1}{\sqrt{2\pi\sigma^2(\theta)}} \cdot \exp\left(- \frac{(\theta_i - \mu(\theta))^2}{2\sigma^2(\theta)} \right) d\theta. \tag{34}$$

In Eq. 34, the distribution of each solid departure-angles is assumed to be normally distributed, with average $\mu(\theta)$ and standard deviation $\sigma(\theta)$. Thus, in Eq. 33, M is computed as the ith root of the product of the probabilities of i solid departure-angles, with i being 2, 4, or 6, depending on whether 1, 2, or 3 groups have violated their NOC limits.

Identification of disturbances

Disturbance 7 is considered to demonstrate the proposed on-line strategy, with the detection performance obtained summarized in Table 7. It takes 7 samples (21 minutes) from the instigation of the disturbance until an outlier appears on the reactor group scores-plane, with departing angles $\theta = 148°$ and $\varphi = 110°$C. On the basis of the disturbance-mapping database and matching computations, the information so far fits Disturbances 1, 2, 6 and 7, with 6 being the most probable fault (Eq. 33 gives a matching coefficient of $M = 0.42$ for Disturbance 6). Two samples later, the separator group data moves out of NOC, with direction angles $\theta = 307°$ and $\varphi = 138°$. Thus, Disturbance 6 is eliminated from further consideration, and the matching for Disturbance 1 drops to 0. Disturbances 7 and 2 are therefore left, with the latter being the more probable ($M = 0.57$). One sample later, the stripper group data deviate from NOC, with angles $\theta = 79°$, $\varphi = 102°$, triggering a further revision of the diagnosis. Disturbance 2 now has a near-zero matching coefficient, while that for Disturbance 7 is up to 0.41, and is deemed to be the most probable disturbance.

Successful identification of the first seven disturbances has been demonstrated. The other programmed disturbances in the TE simulation involve random variation (8–12), slow drifts (13), sticking valves (14 and 15), and unknown disturbances (16–20). In principle, the mapping procedure can be applied to include these cases in the database, although the logging of random changes is rather problematic. These disturbances will cause outliers in two opposing directions in the relevant diagnosis group scores-planes. Careful analysis is required to differentiate these cases from false alarms and unidirectional step changes. The method was successfully applied to the identification of most of the unknown disturbances (17–20), with these uniquely mapped as new disturbances.

Table 7. Disturbance Identification Trajectory for Disturbance 7

Samples			0			2			3
Disturbance	θ_1	φ_1	M	θ_2	φ_2	M	θ_3	φ_3	M
(−) 1	0.22	0.62	0.37	0					
(−) 2	0.30	0.78	0.40	0.80	0.80	[0.57]	0		
(−) 6	0.82	0.22	[0.42]	0					
(+) 7	0.01	0.80	0.09	0.90	0.94	0.29	0.69	0.84	[0.41]

The DAPCA algorithm was tested with the normal data set of the Tennessee Eastman process, with the maximum delay, $d_{\max}$, defined as 1 hour (20 samples). Since this process is operating under closed loop, the partitioning of the variables between inputs and outputs is artificial, since correlation between them exists as a result of feedback. It was found that input variables 1 and 2 (the feed flows of D and E) need to be shifted back by one sample, and variables 8 and 11 (the stripper liquid product flow and the condenser cooling water flow) need to be shifted back by 2 and 5 samples, respectively. As a result of these delay adjustments, V_{NOC} is reduced by about 20%. Examination of diagnosis performance for all step disturbances was carried out in the same manner as for Example 2, but with only one test for each disturbance at its prespecified nominal value (that is, its magnitude was set to one) simulated for 5 h (100 samples). The results, which are presented in Table 8, indicate that only modest improvements are achieved in disturbance isolation capability. It should be mentioned that these results were obtained without invoking SSPCA. For this example, delay adjustment does not add significant improvement over that which can be achieved with SSPCA, which is not surprising for this closed-loop process.

Conclusions

This article has presented an algorithm for detecting and identifying excursions from normal conditions. It shows that

Table 8. Euclidean Distance for Step Disturbances

Disturbance	r	r_{DA}	$(1 - r/r_{DA}) \times 100\%$
1	399	441	11
2	57.9	64.5	11
3	2.28	2.90	27
4	29.0	31.0	6.9
5	1.07	1.11	3.7
6	90.9	93.1	2.4
7	1,780	1,900	6.7

by combining relatively simple preprocessing of the raw data with PCA, more accurate mapping and identification of disturbances can be accomplished. The preprocessing methods exploit the fact that the order of the samples is important, which is neglected by conventional PCA. In SSPCA, the appropriate number of samples to be summed, s, needs to be selected large enough to enable small shifts to be detected, but no larger than necessary to reduce the diagnosis reaction time to a minimum. The strength of the proposed method is apparent especially when small shifts need to be diagnosed and conventional PCA is not adequate. This method was proved effective on both small-scale and large-scale examples, where for the latter there was also a clear definition of a strategy dealing with high-dimensionality systems and ways to handle on-line problems that arise when monitoring continuous processes. In DAPCA, performing optimal shifts increases the correlation between inputs and outputs. Although the idea and its implementation are simple, its usefulness depends on the process dynamics and complexity.

Acknowledgment

This research was supported by the Israel Science Foundation founded by the Academy of Sciences and Humanities. The authors wish to acknowledge the assistance of Prof. N. L. Ricker, who provided access to his MATLAB–FORTRAN interface for the Tennessee-Eastman process simulation. Finally, the helpful comments of the anonymous reviewers are appreciated.

Notation

A = correlation matrix
I = isolation ratio (defined in Eq. 16)
P = matrix of principal component vectors, arranged columnwise (eigenvectors of A)
s = number of recursively summed scores
V_{NOC} = multidimensional volume defining NOC (define in Eqs. 13 and 14)
Y = optimal shifted data array of n rows and m columns
α = degree of sequential correlation
δ = disturbance magnitude
λ_i = the ith eigenvalue of A
Λ = a diagonal matrix of eigenvalues of A
θ = NOC-departure-angle for standard PCA
$\tilde{\theta}$ = NOC-departure-angle for SSPCA

Literature Cited

Allgöwer, F., and A. Ilchmann, "Multivariable Adaptive λ-Tracking for Non-Linear Chemical Processes," *Proc. ECC*, **3**, 1645 (1995).
Downs, J. J., and E. F. Vogel, "A Plant-Wide Industrial Process Control Problem," *Comput. Chem. Eng.*, **17**, 245 (1993).
Dunia, R., and S. J. Qin, "Subspace Approach to Multidimensional Fault Identification and Reconstruction," *AIChE J.*, **44**, 1813 (Aug. 1998).
Georgakis, C., B. Steadman, and V. Liotta, "Decentralized PCA Charts for Performance Assessment of Plant-wide Control Structures," *Proc. Triennial World Cong.* IFAC, Int. Fed. of Automatic Control, San Francisco (1996).
Jackson, J. E., *A User's Guide to Principal Components*, Wiley, New York (1989).
Kosanovich, K., K. S. Dahl, and M. J. Piovoso, "Improved Process Understanding using Multiway Principal Component Analysis," *Ind. Eng. Chem. Res.*, **35**, 138 (1966).
Kramer, M. A., "Nonlinear Principal Component Analysis Using Autoassociative Neural Networks," *AIChE J.*, **37**(2), 233 (1991).
Kresta, J. V., J. F. MacGregor, and T. E. Marlin, "Multivariate Statistical Monitoring of Process Operating Performance," *Can. J. Chem. Eng.*, **69**, 35 (1991).
Ku, W., R. H. Storer, and C. Georgakis, "Disturbance Detection and Isolation by Dynamic Principal Component Analysis," *Chemometrics Intell. Lab. Sci.*, **30**, 179 (1995).
Lewin, D. R., "Predictive Maintenance using PCA," *Control Eng. Pract.*, **3**(3), 412 (1995).
Mardia, K. V., J. Kent, and J. M. Bibbi, *Multivariate Analysis*, Academic Press, London (1982).
Martens, H., and T. Naes, *Multivariate Calibration*, Wiley, New York (1989).
McAvoy, T. J., and N. Ye, "Base Control for the Tennessee Eastman Problem," *Comput. Chem. Eng.*, **18**, 383 (1994).
Montgomery, D. C., *Introduction to Statistical Quality Control*, Wiley, New York (1991).
Ogunnaike, B. A., and W. H. Ray, *Process Dynamics, Modeling and Control*, Oxford Univ. Press, New York (1994).
Raich, A., and A. Cinar, "Statistical Process Monitoring and Disturbance Diagnosis in Multivariable Continuous Processes," *AIChE J.*, **42**, 995 (1996).
Raich, A., and A. Cinar, "Diagnosis of Process Disturbances by Statistical Distance and Angle Measures," *Comput. Chem. Eng.*, **21**, 661 (1997).
Rivera, D. E., S. Skogestad, and M. Morari, "Internal Model Control: 4. PID Controller Design," *Ind. Eng. Chem. Proc. Des. Dev.*, **25**, 252 (1986).
Sanetan, A., G. L. M. Koot, and L. C. Zollo, "Statistical Data Analysis of a Chemical Plant," *Comput. Chem. Eng.*, **21**, 1123 (1997).
Wachs, A., and D. R. Lewin, "Process Monitoring using Model-based PCA," *Proc. of DYCOPS'5, 86-91 Conf.*, Int. Fed. of Automatic Control (1998).
Wachs, A., Y. Rotem, and D. R. Lewin, "Combining PCA with Parallel Coordinates for Process Monitoring," in press (1999).
Wise, B. M., N. L. Ricker, D. F. Veltkamp, and B. R. Kowalski, "A Theoretical Basis for the Use of Principal Component Models for Monitoring Multivariate Processes," *Proc. Control Quality*, **1**, 41 (1990).
Wold, S., P. Geladi, and K. Esbensen, "Multi-Way Principal Components and PLS Analysis," *J. Chemometrics*, **1**, 41 (1987).
Wold, S., "Exponentially Weighted Moving Principal Components Analysis Projections to Latent Structures," *Chemometrics Intell. Lab. Syst.*, **23**, 149 (1994).
Wood, R. K., and M. W. Berry, "Terminal Composition Control of a Binary Distillation Column," *Chem. Eng. Sci.*, **29**, 1707 (1973).
Zhang, J. E., B. Martin, and J. Morris, "Process Monitoring using Non-Linear Principal Component Analysis," *Proc. IFAC World Cong.*, Int. Fed. of Automatic Control, San Francisco (1996).

Manuscript received Nov. 3, 1997, and revision received Feb. 16, 1999.